Stabilized Free-Space Optical Frequency Transfer

D. R. Gozzard,[1,2,*] S. W. Schediwy,[1,2] B. Stone,[2] M. Messineo,[2] and M. Tobar[3]

[1] *International Centre for Radio Astronomy Research, ICRAR M468, The University of Western Australia, 35 Stirling Hwy, Crawley, Western Australia 6009*

[2] *Department of Physics, School of Physics, Mathematics & Computing, The University of Western Australia, 35 Stirling Hwy, Crawley, Western Australia 6009*

[3] *ARC Centre of Excellence for Engineered Quantum Systems, Department of Physics, School of Physics, Mathematics & Computing, The University of Western Australia, 35 Stirling Hwy, Crawley, Western Australia 6009*

(Received 9 April 2018; revised manuscript received 6 June 2018; published 29 August 2018)

The transfer of high-precision optical frequency signals over free-space links, particularly between ground stations and satellites, will enable advances in fields ranging from coherent optical communications and satellite Doppler ranging to tests of General Relativity and fundamental physics. We present results for the actively stabilized coherent phase transfer of a 193-THz continuous-wave optical frequency signal over horizontal free-space links 150 and 600 m in length. Over the 600-m link, we achieve a fractional frequency stability of 8.9×10^{-18} at 1 s of integration time, improving to 1.3×10^{-18} at an integration time of 64 s, suitable for transmission of optical atomic clock signals. The achievable transfer distance is limited by deep fading of the transmitted signal due to atmospheric turbulence. We also estimate the expected additional degradation in stability performance for frequency transfer to Low Earth Orbit.

DOI: 10.1103/PhysRevApplied.10.024046

I. INTRODUCTION

Free-space transfer of phase-coherent signals from optical atomic clocks, particularly between satellites and ground stations, will enable significant improvements in coherent optical communications, time-scale comparisons over intercontinental distances, precision navigation, satellite Doppler ranging, geodesy, tests of General Relativity, and other fundamental physics experiments [1–11]. Free-space links can also offer advantages in cost and flexibility of deployment compared to optical fiber networks [12,13]. However, refractive-index fluctuations of air due to atmospheric turbulence induce phase perturbations on the transmitted optical signals. This degrades the coherence and, therefore, the usefulness of the signals as a scientific and industrial tool [4,14–17]. Active phase-stabilization systems can overcome this degradation and greatly improve the accuracy and precision of the transmitted signals.

Time- and frequency-transfer techniques previously developed for the distribution of high-precision signals over long-distance optical fiber links [18–24] can also be applied to free-space transmission [16]. Two-way time- and frequency-transfer systems employing optical frequency combs at the transmit and receive ends have already demonstrated time and frequency transfer over horizontal links through up to 12 km of atmosphere [12–14] at levels of precision suitable for the synchronization and comparison of optical atomic clocks. A space-based optical atomic clock synchronized using ground-to-space links of such a level of stability will enable measurements of General Relativity and other fundamental physics experiments an order of magnitude more precise than will be achieved by the Atomic Clock Ensemble in Space (ACES) mission [25–27]. However, the size and complexity of optical frequency combs restricts the types of satellites that these systems may be deployed on, thus limiting the range of scientific and industrial applications of such satellites. In contrast, coherent, continuous-wave, frequency-transfer techniques require only relatively simple optics and detection hardware at the remote site and so offer advantages in terms of size, weight, and robustness that are critical to successful deployment of such a system on board a satellite. Optical Doppler ranging to satellites and measurements comparing the time scales of ground- and space-based optical clocks using continuous-wave frequency transfer will also be able to achieve superior precision during the limited measurement window available as an orbiting spacecraft is within view compared with measurements made using two-way time- and frequency-transfer (pulsed) techniques [28,29]. However, coherent frequency transfer with active phase stabilization has so far only been demonstrated over distances of the order of 100 m [30] and then only at microwave frequencies.

*david.gozzard@research.uwa.edu.au

We present results of a simple system for the phase-stabilized transmission of a 193-THz (1550-nm) continuous-wave optical signal over horizontal free-space links 150 and 600 m in length, which are estimated, based on results in Refs. [31,32], to be equivalent to transmission distances of approximately 2.2 and 9 km vertically through the atmosphere. We describe the design of the system's free-space terminals and show that deep fading of the optical signal due to atmospheric turbulence limits the availability of coherent free-space optical transfer links using this system. Adaptive optics systems will be required to achieve reliable operation over horizontal links in excess of 1 km in length.

II. EXPERIMENTAL SETUP

A. Phase-stabilized optical-frequency-transfer system

Phase-stabilized frequency-transfer techniques utilize a round-trip signal through the transmission link to measure and compensate for phase fluctuations that are caused by disturbances on the link. Because of this, stabilized frequency-transfer systems require the transmission link to have a high degree of reciprocity in order to precisely measure the link-induced noise and maximize the suppression of phase fluctuations. The reciprocal behavior of free-space links depends on details of the setup, such as the point-ahead angle, and a thorough analysis of this and other setups is covered in [16]. The experiments presented here transmit across a fixed length of turbulent atmosphere in which time-of-flight, atmospheric scintillation, and fading all exhibit reciprocal behavior [33–35], meaning that high-precision stabilized frequency-transfer techniques are compatible with these free-space links.

The frequency-transfer system used in these experiments is an evolution of the design pioneered by Ma and colleagues [24]. As shown in Fig. 1, a 193-THz (1550-nm) optical signal from a laser passes through a 50:50 splitter where one half of the signal reflects from a Faraday mirror (FM), then back through the 50:50 splitter, and finally falls on a photodetector (PD). This forms the short arm of an imbalanced Michelson interferometer, thereby providing an optical reference signal for the phase-stabilization system, with the long arm of the Michelson interferometer being the optical transmission link. The laser we use in these experiments is an NKT Photonics Koheras X15 with a linewidth of <100 Hz, which provides a coherence length in excess of 950 km, sufficient to ensure that the linewidth of the laser does not affect the link stability performance even for transmissions to lower-altitude Low Earth Orbits. The other half of the laser signal passes through an acousto-optic modulator (AOM) where it is shifted by $+50$ MHz before it is passed to a collimator and beam expander, and is then launched into free space. At the remote site, another beam expander and collimator are used to couple the arriving beam into a single-mode fiber. The received signal is split with one half of the signal being directed to the end user or application. The other half of the signal passes through a second AOM which applies a $+70$-MHz frequency shift. This distinguishes the signal returning from the receiver from other unwanted reflections which can then be filtered out in the electronic domain. The signal then reflects from a FM through the AOM again where it receives an additional $+70$ MHz, and back through the free-space link, returning to the transmitter unit. The signal returning to the transmitter unit passes through the $+50$ MHz servo AOM again and terminates on the PD where it generates a 240-MHz beat with the optical reference. The 240-MHz signal carries the phase fluctuations acquired by the transmitted optical signal. The 240-MHz signal is filtered and mixed with a 240-MHz local oscillator reference and the resulting dc signal is used to steer the frequency applied to the servo AOM to compensate for phase fluctuations on the link.

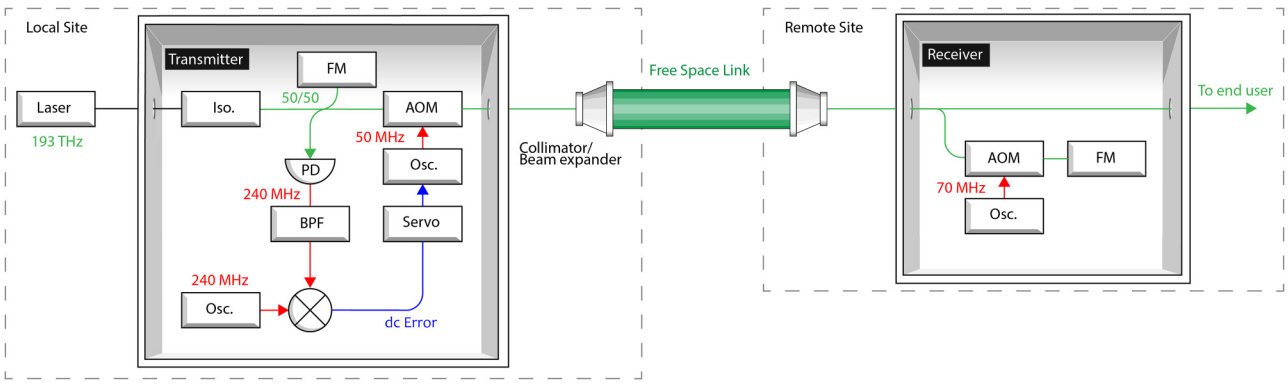

FIG. 1. Free-space phase-stabilized frequency-transfer system. Red paths indicate electronic (radio frequency) connections, green paths indicate optical connections. Iso., isolator; PD, photo-detector; AOM, acousto-optic modulator; Osc., oscillator signal source; BPF, band-pass filter; FM, Faraday mirror.

B. Folded beam link

The architecture of the stabilized frequency-transfer system is intended to have the receiver unit installed in a remote location from the transmitter unit. However, in order to obtain a true measurement of the phase stability of the transmitted signal, the transmitter and receiver must be colocated so that the transmitted and received signals can be compared via an out-of-loop link. This is achieved by "folding" the free-space link using a corner cube reflector as shown in Fig. 2. This means that only one optical terminal is used because the beam reflected by the corner cube reflector returns through the same transmitting optic. A 50:50 fiber splitter is used to couple the transmitter and receiver terminals to the single optic. This greatly simplifies the setup of the test link but has the disadvantage that the transmitted signal loses 3 dB of power with every pass through the splitter, resulting in a total of 12-dB loss that would not be present on an operational free-space link.

The optical signal reaching the receiver unit is combined with an optical reference that was previously split off from the laser signal. The signals terminate on a measurement PD where they produce a 50-MHz signal that is used to measure the stability of the optical transmission. A polarization controller in the remote unit is used to align the polarization of the received light with the polarization of the optical reference from the laser. The 50-MHz signal is directed to an Agilent 53132A Λ-type high-precision frequency counter, which averages the frequency over a 1-s gate time, and separately to a Microsemi 5125A phase noise test set with an acquisition rate of 2 MHz. The output of the counter is logged and used to compute an estimate of the fractional frequency stability of the transmitted signal for both stabilized and unstabilized transmission over the 150- and 600-m horizontal links. The 5125A is used to measure the power spectral density (PSD) of the signal phase noise.

C. Optical terminal design

In operation, two identical free-space optical terminals are required for the frequency-transfer system, one at the transmitter site and one at the receiver site, but because of the folded beam path used in these tests, only one optical terminal is needed. Excluding the effects of atmospheric turbulence, the effective range of the free-space frequency-transfer system will be limited by the optical power loss during transmission due to diffractive losses, extinction losses in the propagation medium, and loss due to coupling into the optical fiber. Because of this, the terminal is designed to be as low loss as reasonably practical.

The size of the terminal optics is determined by the desire to achieve a diffraction-limited beam over the 600-m link, and by the Fried parameter which sets an upper limit on the size of the aperture for which the received light can be efficiently coupled into a single-mode fiber [13,36]. Data from [13] show that an optic of 5 cm in diameter is the largest that would achieve efficient coupling over 600 m in strong turbulence. Therefore, standard 2-in. (5-cm) optics provide a good solution for the design of the optical terminals and will also be useful for future trials over distances of the order of 10 km during moderate to light atmospheric turbulence conditions.

The final terminal design incorporates a fiber-to-free-space collimator that produces a $1/e^2$ intensity radius of 1.12 mm. This beam is directed into a 15:1 beam expander, resulting in a waist with a radius of 16.8 mm and with a divergence of 29 μrad. The beam expander has a nominal aperture of 50 mm, which is reduced to a clear aperture of 48 mm by the mounting hardware. The corner cube reflector (gold-coated for efficient reflection at 1550 nm) has a clear aperture of 50.8 mm. These optics allow us to have diffraction-limited divergence over the whole 600-m atmospheric link, producing a beam $1/e^2$ intensity radius of 24.4 mm returning to the beam-expander aperture.

D. Free-space links

Two free-space links across the University of Western Australia (UWA) campus are used for these experiments (Fig. 3). The stabilized frequency-transfer system and free-space terminal are installed behind a window in an office on the 5th floor of the UWA Physics building (50 m above sea level, approximately 40 m above ground level). The

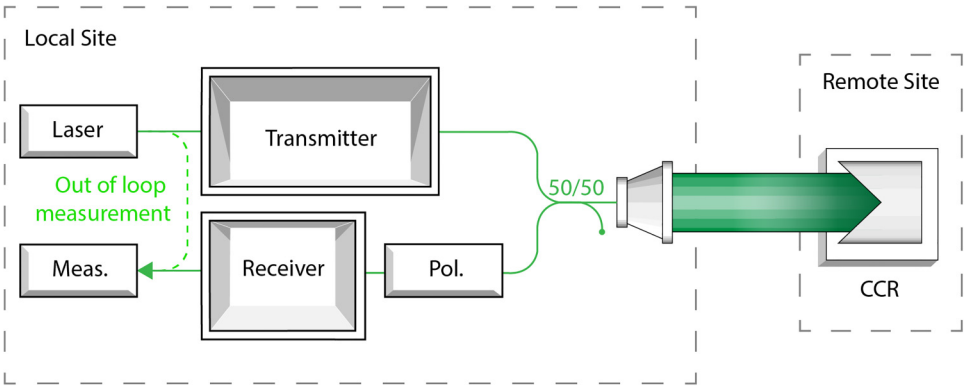

FIG. 2. Folded architecture of experimental free-space link using a corner-cube reflector. CCR, corner-cube reflector; Pol., polarization controller.

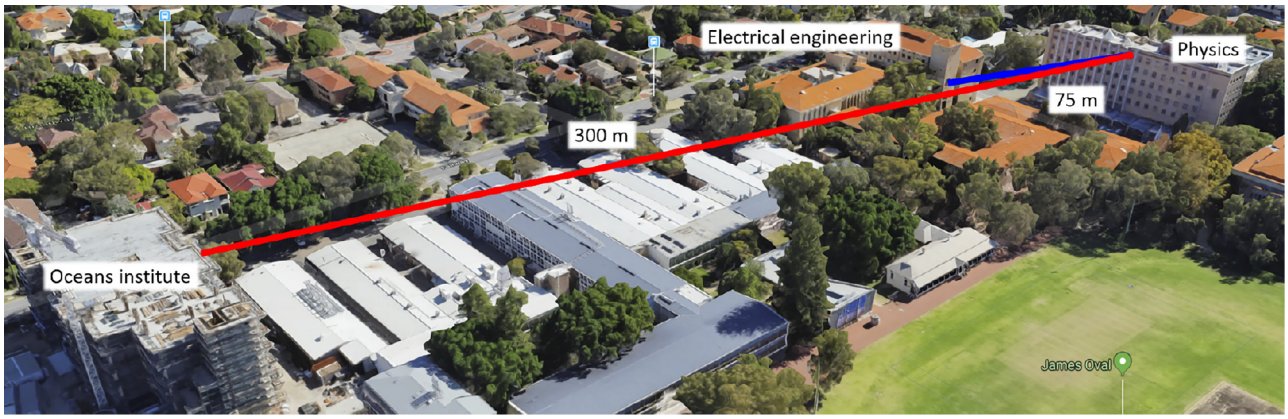

FIG. 3. Beam path from Physics to Electrical Engineering (blue, 75 m) and to the Oceans Institute (red, 300 m). (Modified from Google Maps image.)

corner cube reflector is mounted on a balcony in the Electrical Engineering building 75 m away, creating a 150-m test link, and behind a window at the UWA Oceans Institute building 300 m away, creating a 600-m test link. The link from Physics to Electrical Engineering has a 30° slant propagation path passing over a car park, while the link from Physics to the Oceans Institute is nearly horizontal and passes over a car park and several campus buildings, approximately 25 m above the taller buildings. The link is achieved with both the Physics and Oceans Institute windows closed, which introduces additional attenuation to the transmitted signal.

In both cases, the optical power out of the transmitter unit is +9 dBm (approximately 7.9 mW). This is attenuated by 3 dB through the fiber splitter meaning +6 dBm (approximately 4 mW) is launched into the collimator and beam expander. The coupling loss from fiber to free-space (and vice versa) is 3 dB and the corner cube reflector produces an attenuation of approximately 2 dB due to the accumulation of dust on the mirrors. The beam passes through the window of the Physics office twice, and also twice through the Oceans Institute window for the 600-m link, incurring significant losses upon passing. The expected losses due to scattering and absorption of the 1550-nm light in the air column are approximately 0.5 and 2.5 dB for the 150- and 600-m links, respectively. (This figure assumes attenuation due to the moderate haze typical of this location and time of year and includes a slight clipping of the returning beam for the 600-m link [37,38].) Taking into account the splitter and fiber-coupling losses, the measured loss for the 150-m link to Electrical Engineering is 5.5 dB, while the 600-m link to the Oceans Institute has a loss of 7.5 dB. We attribute the extra 5-dB free-space path power loss to the fact that the beam passes through windows at a significant angle. For the link from Physics to Electrical Engineering, the beam encounters one window at a shallow angle of approximately 30°, while the link to the Oceans Institute passes through two windows at a steeper angle of approximately 75°. Cleaning the Physics window reduces losses by 0.5 dB. We expect some additional parasitic losses in the fiber connectors between the free-space terminal and the power meter. The optical power entering the receiver is then −10.5 dBm (0.09 mW) for the 150-m link and −12.5 dBm (0.06 mW) for the 600-m link. The loss within the receiver unit is 12 dB. After traveling through the link again, and including two passes of the optical splitter, the optical power returning to the transmitter side is −42 dBm (0.063 μW) for the 150-m link and −46 dBm (0.025 μW) for the 600-m link.

It should be noted that the fiber splitter used to connect the transmitter and receiver units to the free-space optic produces a reflection at around −35 dBm that is indistinguishable to the stabilization system from the reflection from the corner cube. The power of this unwanted reflection ultimately determines the limit for the link power loss for this experiment when the system is used in this folded beam path setup. However, this reflection will not be present in normal operation and will not limit the range or performance of an operational stabilization system.

III. RESULTS

The fractional-frequency-stability results computed from the frequency-counter data are shown in Fig. 4. The blue curves with diamond markers represent the stability of the 150-m link, while the red curves with circle markers represent the stability of the 600-m link. The dashed lines with open markers are measurements of the unstabilized frequency transfer and the solid lines with filled markers are the measurements of the stabilized transfer.

The length of the data acquisition for the 600-m link is limited by the magnitude of the atmospheric turbulence. During periods of high turbulence, usually as the ground and buildings heat up in the morning sunlight, scintillation and beam wander of the laser in the atmosphere cause instances of deep fading of the optical power, causing brief

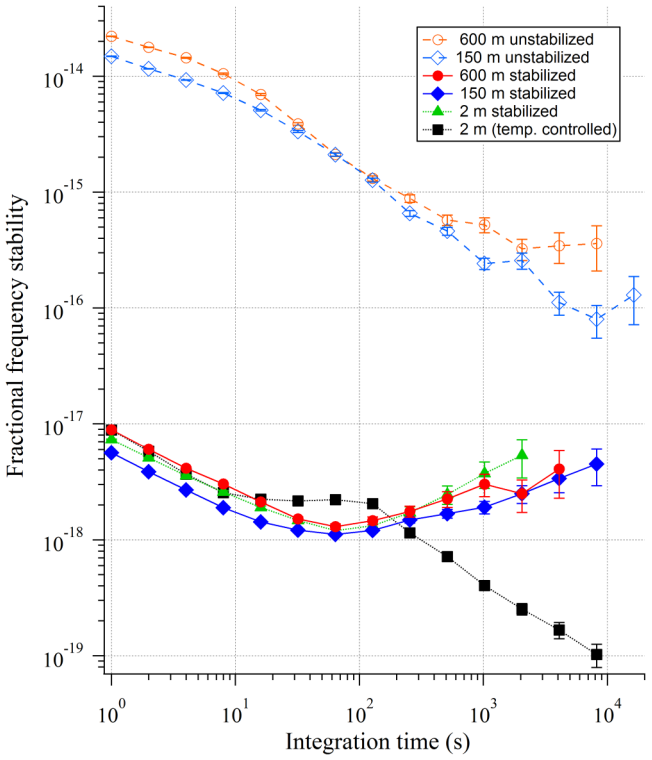

FIG. 4. Fractional frequency stability of the 193-THz optical signal transmitted over 150 m (blue diamonds) and 600 m (red circles). Filled markers with solid lines indicate stabilized transmission. Open markers with dashed lines indicate unstabilized transmission. Black squares, transmission over 2 m in a temperature-controlled laboratory. Green triangles, transmission over 2 m in the Physics building office.

losses of lock and breaks in the frequency-counter data. The measurements presented in Fig. 4 are for the longest break-free period of the data acquisition, about 10 h, during a period when the atmosphere was relatively stable. Each set of measurements, 150 m stabilized, 150 m unstabilized, 600 m stabilized, and 600 m unstabilized, is continued for five days to observe how the performance of the system varies with changing conditions. The results in Fig. 4 are typical of the general performance levels of the system during the testing period. The measured stabilized signal stability varies by a factor of about 2 depending on weather conditions.

Over the 150-m link the stability of the unstabilized transmission is 1.5×10^{-14} at an integration time, τ, of 1 s and integrates down over time. With the stabilization system engaged, the stability improves by more than 3 orders of magnitude, achieving 5.7×10^{-18} at 1 s. The stability improves with a $\tau^{-1/2}$ trend to 1.1×10^{-18} at an integration time of 64 s before becoming degraded at longer integration times, where the trace exhibits a $\tau^{1/2}$ trend.

The unstabilized 600-m transmission has a stability of 2.2×10^{-14} at 1 s and also continues to integrate down over time. The stabilization system improves the stability by more than 3 orders of magnitude, achieving 8.9×10^{-18} at 1 s. Like the 150-m link, the 600-m link exhibits a $\tau^{-1/2}$ trend up to $\tau = 64$ s where it achieves a best stability of 1.3×10^{-18} before the stability degrades at longer integration times, displaying a $\tau^{1/2}$ trend.

Also included in the plot in Fig. 4 are results for the stability of the system over short 2-m free-space test links. The black trace with square markers is for a test performed over 2 m in an air-conditioned metrology laboratory, while the green trace with triangular markers is for a test over 2 m in the unregulated temperature conditions of the unair-conditioned Physics 5th floor office. The results of the 2-m laboratory tests (black squares) show a general $\tau^{-1/2}$ trend up to long integration times, while the results for the 5th floor office (green triangles) exhibit the same change at $\tau = 64$ s as the results from the 150- and 600-m links.

Figure 5 shows plots of the PSDs for the 150- and 600-m links, as well as for a 'zero-length' test achieved by mounting a corner cube reflector directly at the output of the free-space terminal. For both the 150- and 600-m links, the stabilized frequency transfer improves the phase noise by 60 dB at an offset frequency of 0.01 Hz. This tapers to an improvement of 50 dB at 30 Hz for the 150-m link, and 40 dB at 30 Hz for the 600-m link.

IV. DISCUSSION

The fractional frequency results (Fig. 4) show that the stabilized transfer system suppresses the free-space link noise by more than 3 orders of magnitude. Over these atmospheric links, we achieve levels of fractional frequency stability, at integration times less than 64 s, comparable to the best achieved over optical fiber links of comparable length [5,21], and exceed the stability achieved by [12,39] using two-way time and frequency transfer of an optical comb over 2-km atmospheric links by an order of magnitude.

The Agilent 53132A frequency counter used to perform these measurements exhibits an approximately 0.1 s deadtime between each 1 s frequency averaging period which, when successive measurements are juxtaposed in order to average over a longer integration time, biases the expected τ^{-1} slope of the fractional frequency data to $\tau^{-1/2}$ [40–42]. This means that the $\tau^{-1/2}$ trend of the data up to $\tau = 64$ s indicates that the dominant noise process at these shorter integration times is consistent with white phase noise. That the dominant noise process is white phase noise is confirmed using the data from the Microsemi test set. Beyond $\tau = 64$ s, the fractional frequency values increase due to temperature changes, mainly diurnal temperature variations. At these longer time scales, the total fractional-frequency-stability value is a combination of frequency instability due to turbulence and temperature variations, and is also biased by the effects of the dead time of the

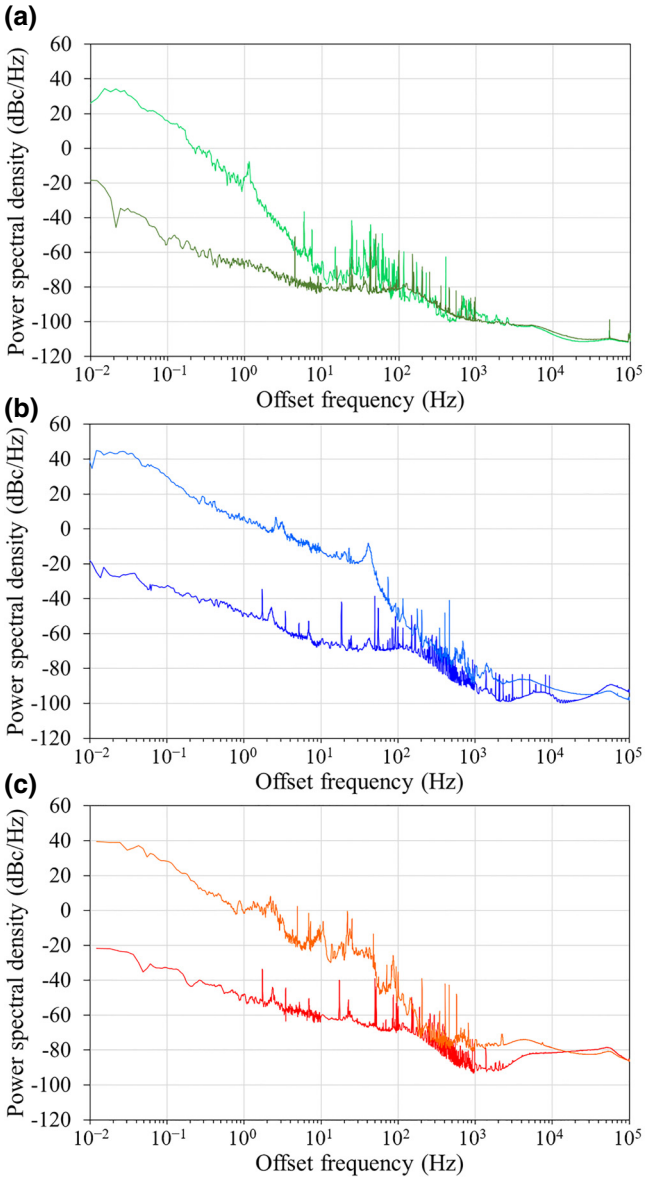

FIG. 5. PSD of 193-THz optical signal transmitted over (a) 0 m, (b) 150 m, and (c) 600 m. Dark green, 0 m stabilized; light green, 0 m unstabilized; dark blue, 150 m stabilized; light blue, 150 m unstabilized; red, 600 m stabilized; orange, 600 m unstabilized.

frequency counter. However, the temperature variations are the dominant noise source.

The results of the short 2-m link tests in the office and the laboratory show that the degradation of the out-of-loop measurement of the fractional frequency stability after 64 s is due to temperature changes within the room in which the tests are performed. The room is an ordinary office with poor temperature stability and no air-conditioning, rather than an air-conditioned laboratory. This means that the out-of-loop measurement system has poor thermal isolation resulting in a degradation of the measured frequency stability at time scales above 64 s. Better thermal isolation of the out-of-loop components will improve the measured performance of the system at longer integration times. From the results of the 2-m tests in the air-conditioned laboratory, we expect the actual stability of the system over the 150- and 600-m links to reach the 1×10^{-19} level by 10^4 s of integration. As this is a free-space frequency-transfer system, the optical terminals will, by necessity, be relatively exposed to the elements in operation. However, because the entire link (long arm of the Michelson interferometer) is stabilized, the stabilization system can be placed in the nearest convenient room with good temperature stability and a fiber patch link can be run to the optical terminal.

The PSD plots for the unstabilized links, Fig. 5, show that the atmosphere is the dominant source of phase noise at offset frequencies from 0.1 Hz to several hundred Hz. Below 0.1 Hz, a large fraction of the phase noise is contributed by mechanical disturbances, including low-frequency vibrations and temperature fluctuations, to the free-space frequency-transfer system. This suggests that, in these tests where the equipment is being used in a relatively noisy room with poor temperature stability, the low-frequency performance of the stabilization system is close to being limited by these mechanical disturbances. The stabilized frequency transfer achieves up to 60-dB improvement in phase noise at low offset frequencies and continues to provide effective suppression at offset frequencies up to several hundred hertz over both the 150- and 600-m links. This is consistent with the atmospheric turbulence model in [36] that predicts that the angle-of-arrival jitter spectrum cuts off sharply at frequencies above $10\ V/2\pi D$ (where V is the wind speed in m/s and D is the aperture diameter in meters). The phase fluctuations at frequencies higher than 1 kHz seen in the plots, frequencies where atmospheric fluctuations are unlikely to have a significant contribution, are most likely due to acoustic frequency mechanical disturbances to the stabilized transfer system and to the fiber patch that delivers the optical signal to the free-space terminal. The increase in phase noise above 1 kHz from zero length, to 150 m, to 600 m is due to the slightly different setups for each measurement. For example, to achieve the 600-m link, the free-space terminal needs to be mounted to a different wall, and has a longer fiber run to it from the stabilization system than for the 150-m link, while the zero-length test is achieved with a corner cube reflector mounted rigidly to the free-space terminal, avoiding any differential motion between the terminal and reflector. The demonstrated suppression of thermal and seismic noise, as well as atmospheric noise, by the stabilized frequency-transfer system shows that the system is capable of handling real-world applications where the equipment may not be installed in ideally quiet environments and the transmitter and receiver units will be subject to differential motion.

The data for the unstabilized links in panels (b) and (c) of Fig. 5 exhibit slopes close to $f^{-8/3}$ between offset frequencies from 0.1 to 50 Hz, consistent with the noise spectrum that would be expected from standard Kolmogorov turbulence theory [4,43]. However, the traces for the unstabilized links in Fig. 4 do not exhibit the corresponding $\tau^{-1/6}$ slope expected from the theory. Instead, the traces exhibit slopes close to $\tau^{-0.36}$ between $\tau = 1$ s and $\tau = 8$ s where they start to exhibit slopes of τ^{-1} until long-period temperature fluctuations begin to dominate at $\tau = 512$ s. This discrepancy between the measured and expected values is due to the effects of dead time in the frequency counter, as well as the dominance of noise due to mechanical perturbations at time scales longer than $\tau = 10$ s as seen in Fig. 5.

The atmosphere is found to be most stable between the times of 5 p.m. and 5 a.m. PSD measurements are obtained during the early evening, with fractional-frequency-stability measurements being left to accumulate data over night until increased atmospheric turbulence in the late morning causes signal fading and a resulting loss of lock and cycle slips. Temperature differentials during the day will create much greater turbulence, to the extent that on fine mornings with little wind, the turbulence is so great that deep fading of the link signal will occur regularly, causing the system to lose lock every few seconds on the 600-m link. On a typical day, the 600-m link will experience less than one cycle slip per hour between 5 p.m. and 5 a.m. The rate of cycle slips will increase to an average of about one cycle slip per minute at midday. Days with extremely bad turbulence can produce a cycle slip every 5 s on average, which can increase still further to one cycle slip per second if it is raining. It is because of these cycle slips that the Agilent 53132A is the device primarily used to obtain the fractional-frequency-stability data, despite exhibiting measurement dead time, because it will continue recording after a cycle slip, whereas the Microsemi 5125A will abort the measurement if a cycle slip or significant signal power reduction occurs. This means that the Agilent device can be used to record the system performance over longer periods of time.

Overall, the stability levels achieved by the system shown in both the PSD and fractional-frequency-stability plots are suitable for applications where comparison between optical atomic clocks is required. However, atmospheric scintillation causing signal fading became so pronounced on the 600-m link that such a link becomes unuseable in adverse turbulence conditions. Because of this, 600 m seems to be near the longest useful horizontal link achievable without the inclusion of adaptive optics systems. Indeed, [14] reported in excess of 100 signal interruptions per second over their 12-km free-space optical link, which would severely limit the availability of coherent frequency-transfer links.

Both [4,12] report that the integrated turbulence across their respective 2- and 5-km links is similar to the integrated turbulence from ground to a satellite. While our longest link is only 600 m, this means we are sampling atmospheric noise with a PSD within an order of magnitude of that expected for a vertical path through the whole atmosphere. The fractional frequency and PSD results reported in Figs. 4 and 5, respectively, show that the performance of the stabilized transfer system is not yet distance limited, so similar performance over longer horizontal and vertical links should be possible with the addition of an adaptive optics system. Extending the system to a 12-km link, equivalent to those achieved by [13,14], we would expect the free-space signal to be exposed to greater phase noise, however, the servo loop bandwidth, which is set by the signal's round-trip time, would still be greater than 10 kHz. From Fig. 5 we see that this reduction in loop bandwidth should not result in a significant increase in the amount of phase noise that is outside the servo bandwidth, and which would not be suppressed by the servo. Therefore, we expect the servo loop to continue to effectively suppress the in-loop phase noise and thus the fractional-frequency-stability performance of an approximately 12-km horizontal link to be similar to the current result.

The optical power budget with the current optical terminals is insufficient to allow stabilized transfer to Low Earth Orbit. Higher initial optical power will extend the range of the present system, and adaptive optics will also enable the use of larger transmitting and receiving optics. Even though the integrated noise on a 12-km horizontal link should be equal to or less than that of a vertical link to Low Earth Orbit, the reduction in feedback bandwidth due to the light round-trip time should begin to impact the achievable stability over the distances involved in transmitting to Low Earth Orbit and beyond.

For an approximately 1000-km link to Low Earth Orbit, the servo bandwidth will be reduced to 150 Hz. As shown in Fig. 5, the dominant phase noise induced by atmospheric fluctuations occurs at frequencies lower than approximately 100 Hz so there will only be a moderate increase in out-of-loop phase noise. This can be compared to the 1100-km stabilized optical frequency transfer via fiber optic link implemented in [44] in which they achieved a fractional frequency stability of 4×10^{-16} at 1 s with a servo bandwidth of 100 Hz (due to the lower speed of light in fiber). However, because the fiber link picks up phase noise along its entire length, unlike a free-space link to orbit in which the majority of the phase noise would be acquired in the first few kilometers, the unstabilized phase noise in [44] is much greater than for a vertical free-space link. [See [44] Fig. 4(b).] We, therefore, expect the fractional frequency performance of stabilized frequency transfer to Low Earth Orbit to remain below the 4×10^{-16} at 1 s value reported by [44].

The coherence length of the laser in these tests is 950 km, but real applications of this technology will use either a cavity-stabilized laser (linewidth <1 Hz) or a laser locked to an optical atomic clock, which will enable phase-stable optical frequency transfer throughout Low Earth Orbit and beyond.

V. CONCLUSION

The stabilized optical-frequency-transfer system in this paper effectively suppresses the phase perturbations induced on the signal by atmospheric turbulence and refractive-index changes, achieving levels of stability over these short distances comparable to the best stabilized fiber links, and exceeding the fractional frequency stability achieved by [12,39] over 2-km free-space links by an order of magnitude for averaging times up to 64 s. By either improving the thermal isolation of the stabilized frequency-transfer system or locating the system in a temperature-stable room away from the optical terminal, we expect the stability performance to continue to integrate down, as in our laboratory-based measurement, over a period of at least several minutes typical of the transit times of satellites in Low Earth Orbit. Work is underway to improve the thermal shielding of the frequency-transfer system.

Taking into account the reduction in servo loop bandwidth and comparing the expected (lower) phase noise of a vertical free-space link with that of an optical fiber link of comparable distance, we expect the fractional frequency performance to Low Earth Orbit to be better than the 4×10^{-16} at 1 s achieved by [44], and to integrate down (at $\tau^{-1/2}$ if using an Agilent 53132A) over a period of several minutes. This makes the system suitable for use in the transmission of optical atomic clocks signals and other high-precision coherent signals. The use of only small size and low complexity components at the receiver makes this system ideally suited for deployment on future spacecraft for ground-to-space optical time scale comparison.

Currently, the practical horizontal transmission distance is limited to about 600 m by deep fading of the optical signal caused by scintillation and jitter in beam angle-of-arrival. To achieve effective and useful transmission of coherent signals over longer distances, adaptive optics systems will be needed to correct the wave-front aberrations that cause this deep fading.

Adaptive optics systems have previously been shown to be compatible with stabilized optical two-way time- and frequency-transfer systems [16,45]. We are currently exploring combining the stabilized frequency-transfer system with adaptive optics. Preliminary results over a 22-m link in the laboratory indicate that adaptive optics systems are compatible with this technique and have been shown to lead to further improvements in fractional frequency stability and noise PSD.

With the inclusion of an adaptive optics system we expect the transfer distance of the system to be limited by the optical power loss due to beam divergence. Under this scenario, the range of the system can be extended by the inclusion of erbium-doped fiber amplifiers (EDFAs) at the terminal sites to compensate for the optical power loss of the long links. EDFAs preserve the reciprocity of the link and have been used effectively in fiber-optic links for the stabilized transmission of optical clock signals [5,21]. Based on results in Refs. [31,32], with the inclusion of an adaptive optics system we expect the current optical terminal design to be able to achieve a stabilized transfer distance on an operational horizontal link of approximately 40 km in clear air, and up to 100 km vertically through the atmosphere. A more powerful laser at the local site or larger optics can be used to improve the link power budget and achievable range. For example, increasing the diameter of the optics by a factor of 2 would increase the effective transfer range (with suitable adaptive optics) to approximately 400 km.

ACKNOWLEDGMENTS

The authors wish to thank Dr. Francis Bennet and Dr. Lyle Roberts for their efforts in enabling the preliminary adaptive optics tests, and Madeleine Sheard for her assistance with this work. This work was supported by the Australian Research Council's Linkage Infrastructure, Equipment and Facilities (Grant No. LE160100045) funding scheme and the Australian Research Council Centre of Excellence in Engineered Quantum Systems (Grant No. CE170100009).

[1] F. Riehle, Optical clock networks, Nat. Photonics **11**, 25 (2017).

[2] T. Takano, M. Takamoto, I. Ushijima, N. Ohmae, T. Akatsuka, A. Yamaguchi, Y. Kuroishi, H. Munekane, B. Miyahara, and H. Katori, Geopotential measurements with synchronously linked optical lattice clocks, Nat. Photonics **10**, 662 (2016).

[3] A. Derevianko and M. Pospelov, Hunting for topological dark matter with atomic clocks, Nat. Phys. **10**, 933 (2014).

[4] K. Djerroud, E. Samain, A. Clairon, O. Acef, N. Man, P. Lemonde, and P. Wolf, Coherent optical link through the turbulent atmosphere, Opt. Lett. **35**, 1479 (2010).

[5] C. Lisdat, G. Grosche, N. Quintin, C. Shi, S. M. Raupach, C. Grebling, D. Nicolodi, F. Stefani, A. Al-Masoudi, S. Dörscher, S. Häfner, J.-L. Robyr, N. Chiodo, S. Bilicki, E. Bookjans, A. Koczwara, S. Koke, A. Kuhl, F. Wiotte, F. Meynadier, et al., A clock network for geodesy and fundamental science, Nat. Commun. **7**, 12443 (2016).

[6] C. Guerlin, P. Delva, and P. Wolf, Some fundamental physics experiments using atomic clocks and sensors, C. R. Phys. **16**, 565 (2015).

[7] C. W. Chou, D. B. Hume, T. Rosenband, and D. J. Wineland, Optical clocks and relativity, Science **329**, 1630 (2010).

[8] P. Delva, J. Lodewyck, S. Bilicki, E. Bookans, G. Vallet, R. Le Targat, P. E. Pottie, C. Guerlin, F. Meynadier, and C. Le Poncin-Lafitte, Test of Special Relativity Using a Fiber Network of Optical Clocks, Phys. Rev. Lett. **118**, 221102 (2017).

[9] R. Bondarescu, M. Bondarescu, G. Hetényi, L. Boschi, P. Jetzer, and J. Balakrishna, Geophysical applicability of atomic clocks: Direct continental geoid mapping, Geophys. J. Int. **191**, 78 (2012).

[10] B. Altschul, Q. G. Bailey, L. Blanchet, K. Bings, P. Bouyer, L. Cacciapuoti, S. Capozziello, N. Gaaloul, D. Giulini, J. Hartwig, and L. Iess, Quantum tests of the Einstein Equivalence Principle with the STE–QUEST space mission, Adv. Space Res. **55**, 501 (2015).

[11] P. Wolf, Ch. J. Bordé, A. Clairon, L. Duchayne, A. Landragin, P. Lemonde, G. Santarelli, W. Ertmer, E. Rasel, F. S. Cataliotti, M. Inguscio, G. M. Tino, P. Gill, H. Klein, S. Reynaud, C. Salomon, E. Peik, O. Bertolami, P. Gi, J. Páramos, et al., Quantum physics exploring gravity in the outer solar system: The SAGAS project, Exp. Astron. **23**, 651 (2009).

[12] F. R. Giorgetta, W. C. Swann, L. C. Sinclair, E. Baumann, I. Coddington, and N. R. Newbury, Optical two-way time and frequency transfer over free space, Nat. Photonics **7**, 434 (2013).

[13] W. C. Swann, L. C. Sinclair, I. Khader, H. Bergeron, J.-D. Desh, and N. R. Newbury, Low-loss reciprocal optical terminals for two-way time-frequency transfer, Appl. Opt. **56**, 9406 (2017).

[14] L. C. Sinclair, W. C. Swann, H. Bergeron, E. Baumann, M. Cermak, I. Coddington, J.-D. Deschênes, F. R. Giorgetta, J. C. Juarez, I. Khader, K. G. Petrillo, K. T. Souza, M. L. Dennis, and N. R. Newbury, Synchronization of clocks through 12 km of strongly turbulent air over a city, Appl. Phys. Lett. **109**, 151104 (2016).

[15] L. C. Sinclair, F. R. Giorgetta, W. C. Swann, E. Baumann, I. Coddington, and N. R. Newbury, Optical phase noise from atmospheric fluctuations and its impact on optical time-frequency transfer, Phys. Rev. A **89**, 023805 (2014).

[16] C. Robert, J. Conan, and P. Wolf, Impact of turbulence on high-precision ground-satellite frequency transfer with two-way coherent optical links, Phys. Rev. A **93**, 033860 (2016).

[17] B. Sprenger, J. Zhang, Z. H. Lu, and L. J. Wang, Atmospheric transfer of optical and radio frequency clock signals, Opt. Lett. **34**, 965 (2009).

[18] S. M. Foreman, K. W. Holman, D. D. Hudson, D. J. Jones, and J. Ye, Remote transfer of ultrastable frequency references via fiber networks, Rev. Sci. Instrum. **78**, 021101 (2007).

[19] O. Lopez, A. Kanj, P.-E. Pottie, D. Rovera, J. Achkar, C. Chardonnet, A. Amy-Klein, and G. Santarelli, Simultaneous remote transfer of accurate timing and optical frequency over a public fiber network, Appl. Phys. B **110**, 3 (2013).

[20] O. Lopez, F. Kéfélian, H. Jiang, A. Haboucha, A. Bercy, F. Stefani, B. Chanteau, A. Kanj, D. Rovera, J. Achkar, C. Chardonnet, P. Pottie, A. Amy-Klein, and G. Santarelli, Frequency and time transfer for metrology and beyond using telecommunications network fibres, C. R. Phys. **16**, 531 (2015).

[21] S. Droste, T. Udem, R. Holzwarth, and T. W. Hänsch, Optical frequency dissemination for metrology applications, C. R. Phys. **16**, 524 (2015).

[22] S. W. Schediwy, D. Gozzard, K. G. Baldwin, B. J. Orr, R. B. Warrington, G. Aben, and A. N. Luiten, High-precision optical-frequency dissemination on branching optical-fiber networks, Opt. Lett. **38**, 2893 (2013).

[23] S. W. Schediwy, D. R. Gozzard, S. Stobie, J. A. Malan, and K. Grainge, Stabilized microwave-frequency transfer using optical phase sensing and actuation, Opt. Lett. **42**, 1648 (2017).

[24] L. Ma, P. Junger, J. He, and J. L. Hall, Delivering the same optical frequency at two places: Accurate cancellation of phase noise introduced by an optical fiber or other time-varying link, Opt. Lett. **19**, 1777 (1994).

[25] K. U. Schreiber, I. Procházka, P. Lauber, U. Hugentobler, W. Schafer, L. Cacciapuoti, and R. Nasca in Frequency Control Symposium Joint with the 22nd EFTF (IEEE International, 2009), pp. 594–599.

[26] K. U. Schreiber, I. Procházka, P. Lauber, U. Hugentobler, W. Schafer, L. Cacciapuoti, and R. Nasca, Ground-based demonstration of the European Laser Timing (ELT) experiment, IEEE Trans. Ultrason. Ferroelectr. Freq. Control **57**, 728 (2010).

[27] K. Bongs, Y. Singh, L. Smith, W. He, D. Świerd, and S. Vogt, Development of a strontium optical lattice clock for the SOC mission on the ISS, C. R. Phys. **16**, 553 (2015).

[28] K. Djerroud, in *Gravitation and Fundamental Physics in Space* (GPhyS Colloquium, 2010).

[29] K. Djerroud, E. Samain, A. Clairon, O. Acef, N. Man, P. Lemonde, and P. Wolf, in International Conference on Space Optics (International Society for Optics and Photonics, 2010), p. 105652P.

[30] S. Chen, F. Sun, Q. Bai, D. Chen, Q. Chen, and D. Hou, Sub-picosecond timing fluctuation suppression in laser-based atmospheric transfer of microwave signal using electronic phase compensation, Opt. Comm. **401**, 18 (2017).

[31] N. Chiodo, K. Djerroud, O. Acef, A. Clairon, and P. Wolf, Lasers for coherent optical satellite links with large dynamics, Appl. Opt. **52**, 7342 (2013).

[32] A. Zilberman, E. Golbraikh, and N. S. Kopeika, Propagation of electromagnetic waves in Kolmogorov and non-Kolmogorov atmospheric turbulence: Three-layer altitude model, Appl. Opt. **47**, 6385 (2008).

[33] J. H. Shapiro, Reciprocity of the turbulent atmosphere, J. Opt. Soc. Am. **61**, 492 (1971).

[34] R. R. Parenti, J. M. Roth, J. H. Shapiro, F. G. Walther, and J. A. Greco, Experimental observations of channel reciprocity in single-mode free-pace optical links, Opt. Express **20**, 21635 (2012).

[35] D. Giggenbach, W. Cowley, K. Grant, and N. Perlot, Experimental verification of the limits of optical channel intensity reciprocity, Appl. Opt. **51**, 3145 (2012).

[36] R. L. Fante, Electromagnetic beam propagation in turbulent media, Proc. IEEE **63**, 1669 (1975).

[37] B. Lacaze, Gaps of free-space optics beams with the Beer-Lambert law, App. Opt. **48**, 2702 (2009).

[38] R. Tyson, *Principles of Adaptive Optics* (CRC Press, Boca Raton, FL, 2010).

[39] J. D. Deschênes, L. C. Sinclair, F. R. Giorgetta, W. C. Swann, E. Baumann, H. Bergeron, M. Cermak, I. Coddington, and N. R. Newbury, Synchronization of Distant Optical Clocks at the Femtosecond Level, Phys. Rev. X **6**, 021016 (2016).

[40] P. Lesage, Characterization of frequency stability bias due to the juxtaposition of time-interval measurements, IEEE Trans. Instrum. Meas. **32**, 204 (1983).

[41] N. D. Faulkner and E. V. I. Mestre, Time domain analysis of frequency stability using nonzero dead-time counter techniques, IEEE Trans. Instrum. Meas. **34**, 144 (1985).

[42] S. T. Dawkins, J. J. McFerran, and A. N. Luiten, Considerations on the measurement of the stability of oscillators with frequency counters, IEEE Trans. Ultrason. Ferroelectr. Freq. Control **54**, 918 (2007).

[43] R. P. Linfield, M. M. Colavita, and B. F. Lane, Atmospheric turbulence measurements with the Palomar testbed interferometer, ApJ **554**, 505 (2001).

[44] N. Chiodo, N. Quintin, F. Stefani, F. Wiotte, E. Camisard, C. Chardonnet, G. Santarelli, A. Amy-Klein, P. Pottie, and O. Lopez, Cascaded optical fiber link using the internet network for remote clocks comparison, Opt. Express **23**, 33927 (2015).

[45] K. Petrillo, M. L. Dennis, J. C. Juarez, E. Baumann, H. Bergeron, I. Coddington, J.-D. Deschênes, F. R. Giorgetta, N. R. Newbury, and W. C. Swann, in Atmospheric Propagation XIII (International Society for Optics and Photonics, 2016), pp. 9833–9838.